Appl. Phys. B 81, 567–576 (2005)
DOI: 10.1007/s00340-005-1913-3

Applied Physics B
Lasers and Optics

L. MA✉
R.K. HANSON

Measurement of aerosol size distribution functions by wavelength-multiplexed laser extinction

Department of Mechanical Engineering, High Temperature Gasdynamics Laboratory, Stanford University, California 94305, USA

Received: 3 March 2005 / Revised version: 7 June 2005
Published online: 19 July 2005 •

ABSTRACT Previous work on the measurement of aerosol size distribution functions (SDFs) by laser extinction mainly relied on light sources from a relatively narrow wavelength range. This paper investigates the potential advantages of extending the extinction method to a general wavelength-multiplexed laser extinction (WMLE) concept by incorporating an arbitrary number of laser sources from a wider wavelength range. This extension improves the sensitivity of SDF measurements over wider aerosol diameter ranges and enables a stable algorithm to invert the extinction data to obtain SDFs. These advantages are illustrated by an example WMLE scheme employing wavelengths in the spectral range from 0.25 to 10 μm to measure SDFs of water aerosols. Application of this approach to other aerosol systems is also considered. The WMLE scheme was found to provide stable determination of a variety of SDFs with Sauter mean diameters ranging from sub-micron to about 10 μm. The sensitivity of such determinations was evaluated to reveal the optimum applicable range of the wavelengths employed. The analyses performed here provide theoretical background and motivation for practical applications of the WMLE concept.

PACS 07.07.Df; 42.25.Fx; 42.62.Cf

1 Introduction

Among all the optical methods for the measurement of aerosol size distribution functions (SDFs), techniques based on Mie extinction remain attractive owing to their relative simplicity in implementation, capability to provide continuous measurement with high temporal resolution, and very limited requirement of optical access. However, most past work on the measurement of SDFs by the extinction method relied on light sources from a relatively narrow wavelength range (usually in the spectral range from the near-UV to the near-IR) [1–5], resulting in two constraints on the performance of SDF measurements. First, the amount of information that can be inferred about the SDFs from extinction measurements is very limited if these measurements are performed at wavelengths within a narrow spectral range. Twomey and Howell [3] found that extinction measurements based on wavelengths from the near-UV to the near-IR allow only one or two independent inferences about the SDFs for droplets with diameter less than 10 μm. Second, extinction measurements in a narrow spectral range limit the sensitivity of the SDF measurements and the applicable range of the extinction method.

The continuing development of laser technologies facilitates the consideration of incorporating wavelengths in a wider spectral range in the extinction method [6, 7]. Here we extend the extinction method to a general wavelength-multiplexed laser extinction (WMLE) concept by incorporating an arbitrary number of wavelengths in a wide spectral range, and investigate the potential advantages brought about by such an extension to overcome the above constraints. An example WMLE scheme utilizing wavelengths ranging from 0.25 to 10 μm was developed for the SDF measurements of water aerosols to illustrate these advantages. Our previous studies have shown that inference of multiple parameters about the SDFs is allowed by extinction measurements performed at well-selected wavelengths in this extended spectral range. This scheme was found to enable determination of a variety of SDFs having Sauter mean diameter ranging from sub-micron to about 10 μm with enhanced sensitivity compared to extinction schemes based on a limited wavelength range. The sensitivity analysis performed here also provides useful guidance for the selection of wavelengths in the WMLE scheme to achieve optimum SDF measurements. Finally, this WMLE concept shows promise to enable a relatively simple and stable inversion of the extinction data to SDFs.

2 Measurement concept

The governing equations for the measurement of SDFs by Mie extinction are as follows:

$$\tau_\mathrm{i} = -\ln\left(\frac{I_\mathrm{t}}{I_0}\right) = \frac{\pi}{4} C_\mathrm{n} L \int_0^\infty Q(\pi D/\lambda_\mathrm{i}, m) f(D) D^2 \mathrm{d}D, \quad (1)$$

✉ Fax: +1-650-723-1748, E-mail: linma@stanford.edu

where τ_i = the extinction by the aerosols at wavelength λ_i; I_0 and I_t = the intensities of incident and transmitted light at wavelength λ_i; C_n = the number density of the aerosols; L = the path length; $Q(\pi D/\lambda_i, m)$ = the extinction coefficient of an aerosol with diameter D at wavelength λ_i; m = the complex refractive index of the aerosols at wavelength λ_i; $f(D)$ = the aerosol size distribution function defined such that $\int_0^\infty f(D)\mathrm{d}D = 1$, and $f(D)\mathrm{d}D$ represents the probability that an aerosol has diameter between D and $D + \mathrm{d}D$.

The determination of the SDFs then reduces to a solution of Eq. (1) for $f(D)$ based on extinction measurements performed at selected wavelengths. However, Eq. (1) is ill conditioned and the development of a stable algorithm to invert the extinction measurements to SDFs has long been a subject of research effort [1, 6–8]. These algorithms can be divided into two categories. In the first category, no a priori information about the sought SDF is available; and, in the second category, some a priori information is available (for example, the SDF can be described by an empirical distribution function). When the sought SDF can be described by a known function, $f(D)$, Eq. (1) can be modified to the following equation*:

$$R_{ij} = \frac{\tau_i}{\tau_j} = \frac{\bar{Q}(\lambda_i, D_{32})}{\bar{Q}(\lambda_j, D_{32})}, \tag{2}$$

where R_{ij} is the ratio between measured extinction at wavelengths λ_i and λ_j. $\bar{Q}$ and D_{32} are the mean extinction coefficient and Sauter mean diameter defined in Eqs. (3) and (4) respectively:

$$\bar{Q}(\lambda_i, D_{32}) = \frac{\int_0^\infty Q(\pi D/\lambda_i, m) f(D) D^2 \mathrm{d}D}{\int_0^\infty f(D) D^2 \mathrm{d}D}, \tag{3}$$

$$D_{32} = \frac{\int_0^\infty f(D) D^3 \mathrm{d}D}{\int_0^\infty f(D) D^2 \mathrm{d}D}. \tag{4}$$

The log-normal function, as defined in Eq. (5), is one of the most commonly used SDFs and will be used as an example distribution function to introduce the measurement concept:

$$f(D) = \frac{1}{\sqrt{2\pi} D \ln\sigma} \exp\left[-\frac{1}{2(\ln\sigma)^2}(\ln D - \ln \bar{D})^2\right], \tag{5}$$

where σ characterizes the distribution width and $\bar{D}$ the mean size of the distribution. Application of the WMLE to other distribution functions will be discussed in Sect. 6. Figure 1 shows four log-normal distribution functions having the same D_{32} with σ varied over a relatively wide range. It can be seen from Fig. 1 that the diameter spans a decade at a σ of 1.6. In Fig. 2, the mean extinction coefficients ($\bar{Q}$'s) of water aerosols at a temperature of 22°C following log-normal distributions with the σ's shown in Fig. 1 are calculated and compared to the extinction coefficients of a mono-dispersed distribution ($\sigma = 1$). Refractive indices used in the calculations are from Refs. [9, 10] and are listed in the caption of Fig. 2. Figure 2 illustrates that $\bar{Q}$ for a log-normal distribution with a σ of 1.1 has an almost identical profile as that of a mono-dispersed distribution, especially at long wavelengths such as 10 μm. At relatively short wavelengths (e.g. 0.5 and 4 μm), the difference is in the fine ripple structures. This similar profile indicates

*Due to symmetry, $\lambda_i > \lambda_j$ is assumed in this work.

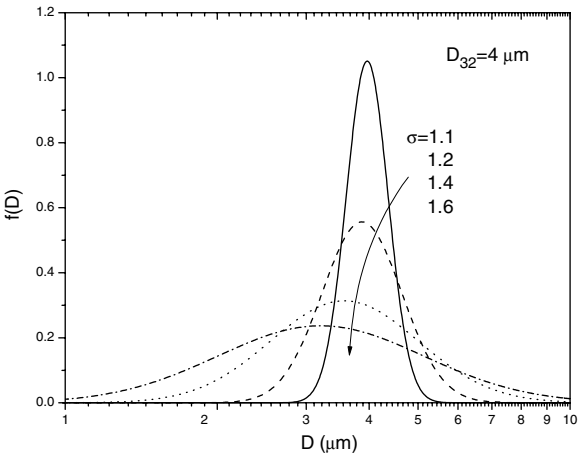

FIGURE 1 Log-normal distribution functions with $D_{32} = 4$ μm and different distribution widths

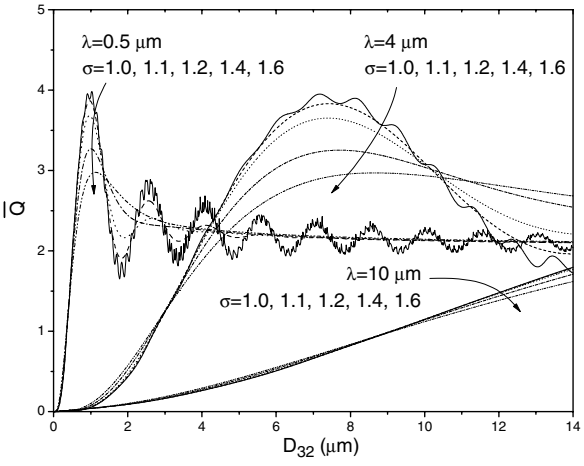

FIGURE 2 $\bar{Q}$ at different wavelengths for water aerosols at a temperature of 22°C following log-normal distributions with various distribution widths. Refractive indices are taken to be $m = 1.335$ at $\lambda = 0.5$ μm, $m = 1.351 - 0.0046\mathrm{i}$ at $\lambda = 4$ μm, and $m = 1.218 - 0.0508\mathrm{i}$ at $\lambda = 10$ μm

that an attempt to distinguish log-normal distributions with σ around 1.1 or less from a mono-dispersed distribution by the extinction method requires measurements at very high accuracy to resolve the fine structures in the extinction-coefficient curves. Therefore, here we limit our consideration for σ in the range of 1.2 to 1.6; the extension to wider ranges of σ will be discussed later in this paper.

Different methods with various levels of complexity have been created to solve Eq. (2) [1, 5, 11] to yield a stable solution of SDFs within certain ranges of mean diameter and distribution width. Observations made in Fig. 2 inspire a relatively simple method to determine SDFs based on extinction measurements. As shown in Fig. 2, $\bar{Q}$ at 10 μm exhibits insensitivity to the distribution width for D_{32} in the range up to 11 μm, and so does $\bar{Q}$ at 0.5 μm for D_{32} greater than about 3 μm. As a result, the ratio defined in Eq. (2) between these two wavelengths will not be sensitive to the distribution width for D_{32} ranging from 3 to 11 μm. Thus, information about D_{32} in this range can be extracted from extinction measurements at these two wavelengths in the absence of detailed knowledge about the distribution width. This observation can be

generalized to other combinations of wavelengths by analyzing the definition of $\bar{Q}$ in Eq. (3). It can be shown that $\bar{Q}$ defined in Eq. (3) is independent of $f(D)$ when Q is a linear function. This analysis provides a mathematical explanation for the insensitivity of $\bar{Q}$ at 10 μm for D_{32} up to 11 μm, because Q at 10 μm behaves almost linearly in this diameter range. It is obvious that $\bar{Q}$ defined in Eq. (3) is also independent of $f(D)$ when Q is a constant. This explains the insensitivity of $\bar{Q}$ at 0.5 μm for D_{32} greater than 3 μm, because Q at 0.5 μm is asymptotic to a constant in this range. Therefore, for any two given wavelengths, when Q at each wavelength meets one of these two conditions (Q can be approximated by a linear function or a constant) over a common D_{32} range, the ratio defined in Eq. (2) between these two wavelengths is insensitive to the distribution width and can be used to determine D_{32} without knowledge about the distribution width in this D_{32} range.

After D_{32} is measured, information about the distribution width (σ) can be obtained by extinction measurements at wavelengths which exhibit a sensitive dependence on the distribution width. For example, $\bar{Q}$ at 4 μm exhibits sensitivity to the distribution width for 4 μm $< D_{32} <$ 10 μm but $\bar{Q}$ at 0.5 μm does not; therefore, the ratio of extinction measurements between these two wavelengths should be sensitive to σ and can be used to measure the distribution width in this diameter range. Measurements of the distribution width in other D_{32} ranges can be obtained by incorporation of other wavelengths.

Finally, D_{32} of a log-normal distribution is related to the parameters of the distribution by

$$\ln \bar{D} = \ln D_{32} - \frac{5}{2}(\ln \sigma)^2. \tag{6}$$

Therefore, $\bar{D}$ is determined after D_{32} and σ are determined, and so is the distribution function.

In Sects. 3 and 4, we discuss the application of the above method to measure D_{32} and the distribution width of log-normal distributions in greater detail, and evaluate the sensitivity of such measurements.

3 D_{32} measurement

As discussed in Sect. 2, D_{32} can be measured by a combination of two wavelengths in the range over which the ratio of $\bar{Q}$ at these wavelengths displays insensitivity to the distribution width (σ). In Fig. 3, the ratio of $\bar{Q}$ shown in Fig. 2 at 0.5 and 10 μm is calculated at three distribution widths ranging from 1.2 to 1.6. As expected, this ratio exhibits overall insensitivity to σ for D_{32} up to about 11 μm and therefore enables D_{32} measurements in this range. For example, when the ratio of extinction between these two wavelengths is measured to be 0.3, D_{32} can be determined to be about 6.8 μm without detailed knowledge of σ. However, closer observation of Fig. 3 as shown in the inset reveals that ambiguity exists in the determination of D_{32} due to the lack of detailed knowledge of σ, especially in the D_{32} range where R, the ration between measured extinction at different wavelengths as defined in Eq. (2), shows more significant variations with σ (such as in the range of $D_{32} >$ 12 μm). Therefore, we need to quantify the ambiguity in the D_{32} measurement to specify

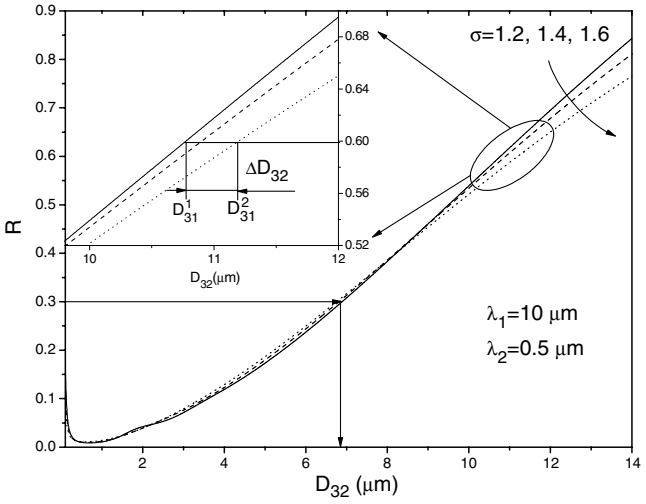

FIGURE 3 Ratio between $\bar{Q}$ at 0.5 and 10 μm shown in Fig. 2 at three distribution widths. The *inset* illustrates the ambiguity (ΔD_{32}) in D_{32} determination due to the lack of detailed knowledge about the distribution width

the applicable range of a given pair of wavelengths and to estimate the measurement uncertainty. As illustrated in the inset of Fig. 3, the largest ambiguity occurs when the actual distribution has a σ of 1.2 (the lower limit of the σ under consideration), while the R value calculated at a σ of 1.6 (the upper limit of the σ under consideration) is used to determine D_{32}, or vice versa. Denote the D_{32} determined by the R value calculated at the lower limit of the distribution width D_{32}^1, and that determined at the upper limit D_{32}^2. Then, the difference between D_{32}^1 and D_{32}^2 (ΔD_{32}) as shown in Eq. (7) represents the largest possible ambiguity in the D_{32} measurement:

$$\Delta D_{32} = D_{32}^1 - D_{32}^2. \tag{7}$$

The relative ambiguity is usually of more interest in most applications. Therefore, the average of D_{32}^1 and D_{32}^2 (D_{32}^{avg}) is used to approximate D_{32} and the ratio between ΔD_{32} and D_{32}^{avg} defined in Eq. (8) is used to quantify the relative ambiguity in D_{32} measurement:

$$\frac{\Delta D_{32}}{D_{32}} \cong \frac{\Delta D_{32}}{D_{32}^{\text{avg}}} = \frac{D_{32}^1 - D_{32}^2}{\left(D_{32}^1 + D_{32}^2\right)/2}. \tag{8}$$

Figure 4 shows the calculation of $\Delta D_{32}/D_{32}$ when the extinction measurements at 0.5 and 10 μm are used to determine D_{32} of water aerosols following log-normal distributions. Figure 4 indicates that D_{32} can be determined within 5% in the range from about 3.4 to 11.7 μm for σ in the range of $1.2 < \sigma < 1.6$ by these two wavelengths. Obviously, better knowledge of σ (i.e. a narrower range of possible σ) reduces the ambiguity in D_{32} measurement or extends the range over which D_{32} can be determined within a fixed level of ambiguity, as demonstrated by the calculation performed for σ in the ranges of 1.2 to 1.4 and 1.4 to 1.6. Note that Fig. 4 also shows that $\Delta D_{32}/D_{32}$ is minimized at 8 μm $< D_{32} <$ 10 μm, a region where the $\bar{Q}$ curves at 10 μm corresponding to different distribution widths intersect as shown in Fig. 2.

Similar methods can be used to determine D_{32} in other ranges. This concept is illustrated through the following example design of a WMLE scheme. Assume the availability of

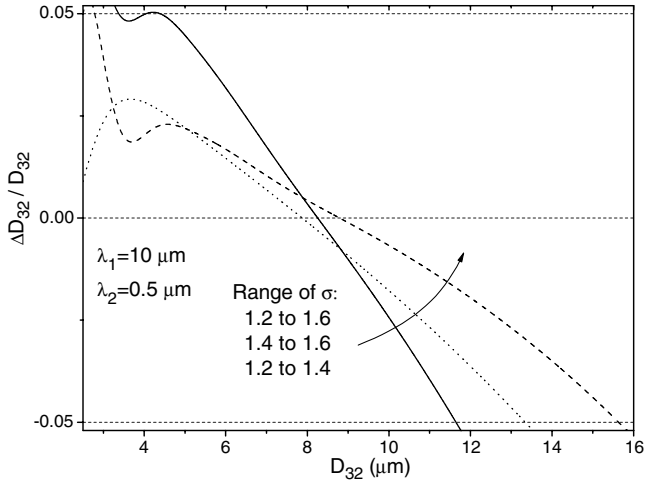

FIGURE 4 Ambiguity in the determination of D_{32} ($\Delta D_{32}/D_{32}$) by the R curves shown in Fig. 3 for different ranges of distribution widths to specify the applicable range for the wavelength combination of 0.5 and 10 μm for D_{32} measurements

light sources with wavelengths ranging from 0.25 to 10 μm to determine D_{32} within 5% in the range of 1 μm $< D_{32} <$ 10 μm for water aerosols following log-normal distributions with $1.2 < \sigma < 1.6$ (at the same time, the number of wavelengths required should be minimized). Forty wavelengths uniformly spaced between 0.25 and 10 μm (the spacing is 0.25 μm) are considered in this design. As shown in Fig. 4, a combination of wavelengths of 0.5 and 10 μm satisfies all the requirements for 3.4 μm $< D_{32} <$ 11.7 μm. Additional wavelengths need to be selected to measure D_{32} in the range of 1 μm $< D_{32} <$ 3.4 μm. This selection is virtually a trial-and-error process, though the analyses performed in Sect. 2 to predict the behavior of $\bar{Q}$ provide insights into this process and substantially reduce the number of trials. The results of the wavelengths selected are summarized in Fig. 5, with the combination of wavelengths of 0.5 and 10 μm to measure D_{32} in the range of 3.4 μm $< D_{32} <$ 11.7 μm, 0.5 and 4 μm to measure 1.5 μm $< D_{32} <$ 3.4 μm, and a pair of relatively short wavelengths, 0.25 and 1.5 μm, to measure 0.7 μm $< D_{32} <$ 1.5 μm. A WMLE scheme based on these five wavelengths satisfies all the requirements of this design. In practice, other criteria may also require consideration. For example, R between the selected wavelengths should behave monotonically in the corresponding D_{32} range to allow unique determination of D_{32}, the value of R should be between 0.1 and 10 to ensure an optimum signal to noise ratio of the measurements, and D_{32} should be measured with a reasonably high sensitivity (S_D) as defined by

$$S_D = \left| \frac{dR/R}{dD_{32}/D_{32}} \right|_\sigma . \tag{9}$$

Calculations show that the above WMLE scheme also satisfies these additional criteria with a S_D greater than unity for $1.2 < \sigma < 1.6$.

Hence, in summary, a WMLE scheme composed of five wavelengths, 0.25, 0.5, 1.5, 4, and 10 μm, will enable sensitive and unique determination of D_{32} in the range of 0.7 μm $< D_{32} <$ 11.7 μm within 5% in the absence of detailed knowledge about σ for water aerosols following log-normal distributions with σ in the range from 1.2 to 1.6. More wavelengths in and beyond this interval would of course enhance the measurement accuracy, and would accommodate expansions in the ranges of D_{32} and σ.

4 Distribution width measurement

As mentioned in Sect. 2, after D_{32} is measured, σ can be determined by a combination of two wavelengths in the D_{32} range where R between these wavelengths exhibits sensitivity to σ. For example, Fig. 2 shows that $\bar{Q}$ at 4 μm is sensitive to the distribution width for D_{32} in the range of 4 μm $< D_{32} <$ 10 μm while $\bar{Q}$ at 0.5 μm is not in this D_{32} range. Therefore, R between these two wavelengths should be sensitive to σ for D_{32} in the range from 4 to 10 μm, as confirmed by the calculations shown in Fig. 6. Figure 6 shows the ratios of $\bar{Q}$ between these two wavelengths for water aerosols following log-normal distributions with various distribution widths. According to Fig. 6, the R curves vary substantially with σ for D_{32} in the range of 4 μm $< D_{32} <$ 10 μm (especially

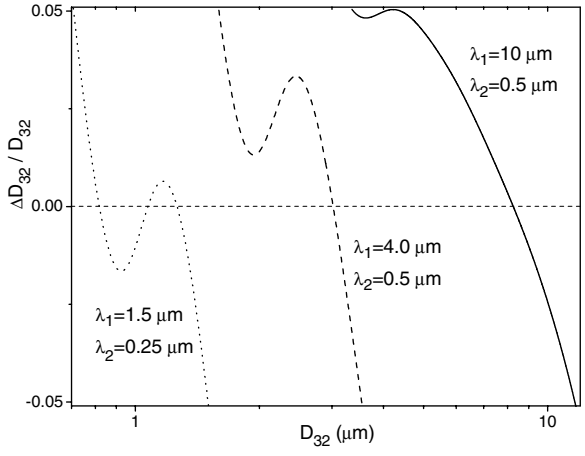

FIGURE 5 Wavelengths selected in the WMLE scheme for the measurement of D_{32} of water aerosols following log-normal distributions with distribution widths ranging from 1.2 to 1.6

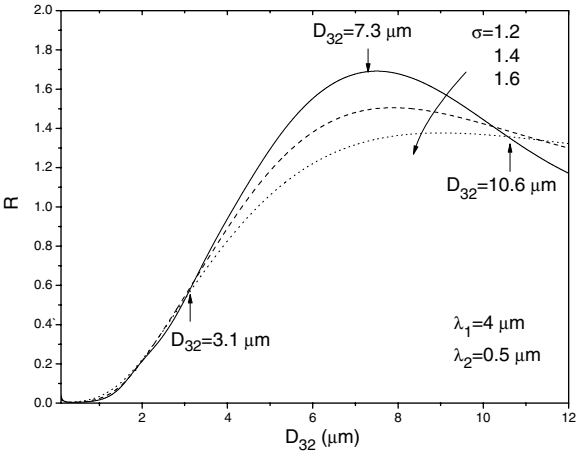

FIGURE 6 Ratio between $\bar{Q}$ at 0.5 and 4 μm shown in Fig. 2 at three distribution widths to illustrate that R shows different sensitivities to the distribution width over different ranges of D_{32}

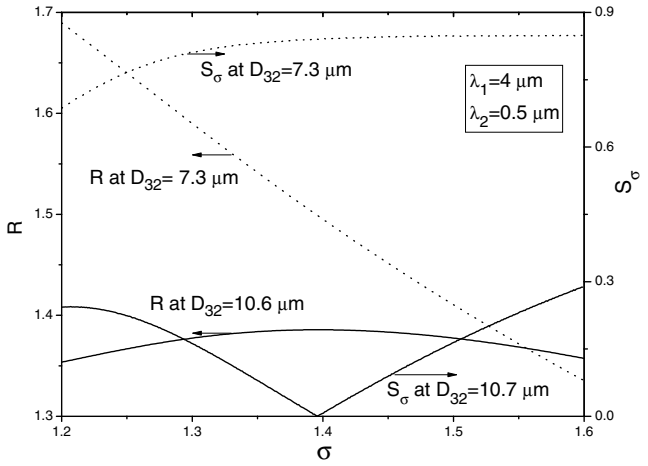

FIGURE 7 Variations of R between $\bar{Q}$ at 0.5 and 4 μm shown in Fig. 2 at two selected D_{32}'s for distribution widths in the range of 1.2 to 1.6 and the sensitivity analysis of this ratio for distribution width measurements

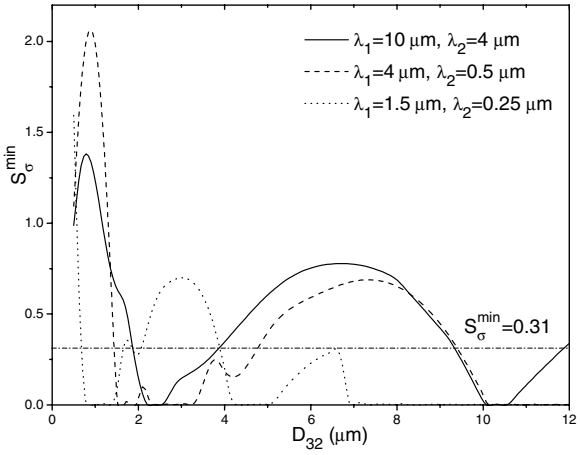

FIGURE 8 Calculations of $\bar{Q}$ for wavelengths selected in the WMLE scheme to specify the applicable D_{32} ranges of different wavelength combinations for σ measurement with optimized sensitivity

in the vicinity of $D_{32} = 7.3\,\mu\text{m}$) and less significantly in other D_{32} ranges (especially in the vicinities of $D_{32} = 3.1$ and 10.6 μm, where the R curves corresponding to different distribution widths intersect).

A quantified evaluation of the sensitivity of R to σ is necessary before applying these wavelengths to measure distribution widths. Variations of R with σ are calculated at selected D_{32}'s mentioned in Fig. 6 and shown in Fig. 7 to provide insights into the quantification of the sensitivity for σ measurements. As expected, the R curve is considerably more sensitive to σ at $D_{32} = 7.3\,\mu\text{m}$ than at $D_{32} = 10.6\,\mu\text{m}$. Moreover, the R curve at $D_{32} = 10.6\,\mu\text{m}$ does not behave monotonically with σ and, consequently, cannot yield a unique determination of σ at this D_{32}. A quantity (S_σ) defined in Eq. (10) provides a measure of the sensitivity and helps to recognize this nonmonotonic behavior:

$$S_\sigma = \left| \frac{\mathrm{d}R/R}{\mathrm{d}\sigma/\sigma} \right|_{D_{32}}. \tag{10}$$

A large S_σ implies that a small proportional change in σ results in a large proportional change in R at the given D_{32}; therefore, sensitive determination of σ is enabled at this D_{32}, and vice versa. If a S_σ of zero occurs, it typically implies that the corresponding R curve is not monotonic at the given D_{32} over the σ range under consideration. As illustrated in Fig. 7, in the σ range from 1.2 to 1.4, S_σ corresponding to $D_{32} = 7.3\,\mu\text{m}$ is greater than 0.6 while S_σ corresponding to $D_{32} = 10.6\,\mu\text{m}$ is less than 0.3. Therefore, the ratio of $\bar{Q}$ between these two wavelengths allows more sensitive determination of σ at $D_{32} = 7.3\,\mu\text{m}$ than at $D_{32} = 10.6\,\mu\text{m}$. Moreover, the S_σ curve at $D_{32} = 7.3\,\mu\text{m}$ has a zero value near $\sigma = 1.4$, which implies that the corresponding R curve is not monotonic and cannot provide a unique determination of σ at this D_{32}. In summary, Fig. 7 shows that the wavelength combination of 0.5 and 4 μm provides sensitive and unique determination of σ at D_{32} near 7.3 μm, but application of this wavelength combination at D_{32} near 10.6 μm results in low sensitivity and ambiguity of the σ determination.

However, generalization of the above discussion is limited because the S_σ defined in Eq. (10) depends on multiple variables (D_{32} and σ). In order to reduce the number of dimensions in the evaluation of S_σ, we define $S_\sigma^{\min}$ as the minimum of S_σ in the range of σ under consideration at a given D_{32}, and use $S_\sigma^{\min}$ to represent the sensitivity of σ measurement at this D_{32}. Clearly, $S_\sigma^{\min}$ is a conservative estimation of the sensitivity for σ measurements, though it still contains the information to help recognize the nonmonotonic behavior of the R curve. Figure 8 shows the calculation of $S_\sigma^{\min}$ for the wavelength combination of 0.5 and 4 μm for distribution widths ranging from 1.2 to 1.6. As expected from Figs. 6 and 7, this $S_\sigma^{\min}$ curve peaks near $D_{32} = 7.3\,\mu\text{m}$ and has zero values near $D_{32} = 3.1\,\mu\text{m}$ and $D_{32} = 10.6\,\mu\text{m}$. For a preset minimum sensitivity requirement, the applicable range of this wavelength combination for σ measurement can be decided by the calculation of $S_\sigma^{\min}$ shown in Fig. 8. For example, if a $S_\sigma^{\min} \geq 0.31$ is required, then according to Fig. 8 the wavelength combination of 0.5 and 4 μm can be applied for σ measurements in the ranges of $0.4\,\mu\text{m} < D_{32} < 1.4\,\mu\text{m}$ and $4.7\,\mu\text{m} < D_{32} < 9.5\,\mu\text{m}$. Figure 8 also presents the $S_\sigma^{\min}$ calculations for two other wavelength combinations (10 and 4 μm, and 1.5 and 0.25 μm). According to our calculations, among all the possible combinations between the wavelengths selected for D_{32} measurements in Sect. 3, these two pairs of wavelengths (10 and 4 μm, and 1.5 and 0.25 μm) provide the optimum σ measurements for D_{32} in the range from 0.4 to 9.5 μm for σ in the range of $1.2 < \sigma < 1.6$. More specifically, as shown in Fig. 8, the wavelength combination of 1.5 and 0.25 μm enables measurements of σ for D_{32} in the range of $1.8\,\mu\text{m} < D_{32} < 3.9\,\mu\text{m}$, the wavelength combination of 10 and 4 μm for $0.4\,\mu\text{m} < D_{32} < 1.8\,\mu\text{m}$ and $3.9\,\mu\text{m} < D_{32} < 9.5\,\mu\text{m}$, and the minimum sensitivity for the σ measurements is greater than 0.31 for σ in the range of 1.2 to 1.6. These two wavelength combinations are also examined to confirm that they satisfy the requirement of $0.1 < R < 10$. Similar to the discussion for D_{32} measurements, additional wavelengths are needed if a higher $S_\sigma^{\min}$ is required or the ranges of D_{32} and σ to be measured are expanded. As mentioned before, Fig. 8 also implies that the incorporation of wavelengths from a wide spectral range expands the applicable range of the extinction method and enhances the sensitivity

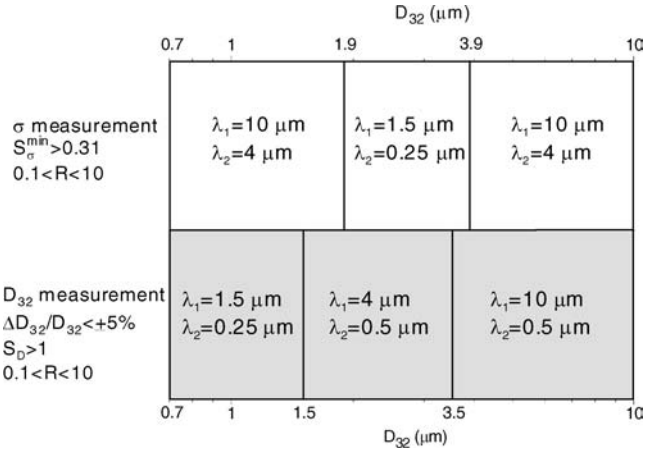

FIGURE 9 Summary of the wavelengths selected in the WMLE scheme to measure SDFs of water aerosols following log-normal distributions, the applicable D_{32} range for each of the wavelength combinations, and the criteria considered in the wavelength-selection process

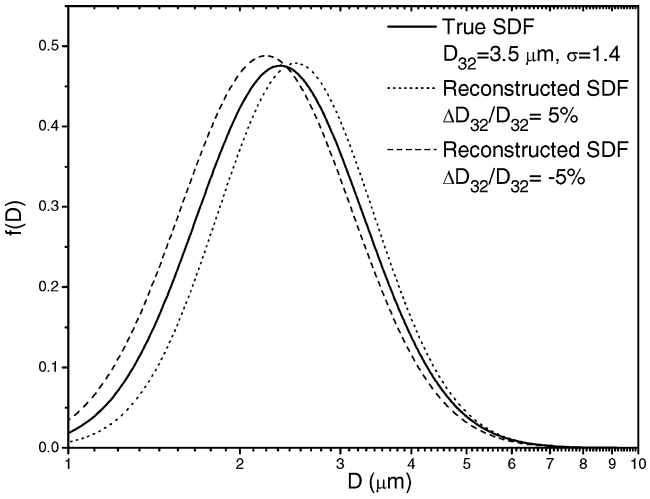

FIGURE 10 Uncertainty analysis for SDF measurements by the WMLE scheme described in Fig. 9

of SDF measurements. For example, in an extinction scheme where only wavelengths in the range of 0.25 to 1.5 μm are utilized, the measurements of SDFs with D_{32} above about 4 μm would be difficult, and the limited wavelength range also impairs the sensitivity of the measurements.

Figure 9 summarizes all the wavelengths selected in Sects. 3 and 4 for the WMLE scheme to measure SDFs of water aerosols following log-normal distributions, the applicable D_{32} ranges for each of the wavelength combinations for optimized SDF measurements, and all the criteria considered in the wavelength-selection process. This scheme enables determination of log-normal distribution functions in the ranges of $0.7\,\mu\text{m} < D_{32} < 9.5\,\mu\text{m}$ and $1.2 < \sigma < 1.6$ with good sensitivity ($S_\text{D} > 1.0$ and $S_\sigma^\text{min} > 0.31$) and signal to noise ratio ($0.1 < R < 10$). According to our previous studies, extinction measurements at these selected wavelengths are mutually independent and therefore do not contain experimental redundancy. Moreover, the method used in this scheme to invert extinction measurements to SDFs is inherently stable. Uncertainties in the SDF measurements are derived from the ambiguity in D_{32} measurements ($\Delta D_{32}/D_{32}$), which is bounded, and the bounds can be estimated based on the calculations shown in Fig. 5. For example, at a D_{32} of 3.5 μm, as shown in Fig. 5, application of the wavelength combination of 4 and 0.5 μm results in a ΔD_{32} that is -5% of the D_{32} to be measured, and application of the combination of 10 and 0.5 μm results in a ΔD_{32} that is 5% of the D_{32} to be measured. These uncertainties in the D_{32} measurement will cause uncertainties in the σ measurements and calculations show that the uncertainties in the σ measurements are less than 2%. Figure 10 shows the results of the uncertainty evaluations at a distribution width of 1.4 and compares the reconstructed distribution functions with the 'true' distribution, which is a log-normal distribution with $D_{32} = 3.5\,\mu\text{m}$ and $\sigma = 1.4$. These two reconstructed distribution functions represent the bounds of the uncertainties for the SDF measurements by the WMLE scheme described in Fig. 9 for $D_{32} = 3.5\,\mu\text{m}$ and $\sigma = 1.4$. Similar results were obtained for other distribution widths. Furthermore, ambiguity in D_{32} measurements ($\Delta D_{32}/D_{32}$) will not exceed that in the case of $D_{32} = 3.5\,\mu\text{m}$ (and similarly $D_{32} = 1.5\,\mu\text{m}$), where D_{32} could be determined by different wavelength combinations with ΔD_{32} having opposite signs.

The current availability of laser sources in a wide spectral range from deep UV to the IR supports the feasibility of the WMLE concept depicted in Fig. 9. For example, a large group of gas lasers operate across the wavelength range from about 200 nm to 12 μm. The most commonly used devices in this group include lasers based on helium–neon (He-Ne), argon (Ar), and carbon dioxide (CO_2). The He-Ne laser can generate wavelengths including 0.5435, 0.6328, 1.523, and 3.391 μm. The Ar-ion laser can generate wavelengths shorter than the He-Ne laser, such as 257, 488, and 514 nm. The CO_2 laser lases at longer wavelengths ranging from 9.2 to 11.4 μm and from 4.6 to 5.8 μm when frequency doubled. Therefore, these primary types of gas lasers can provide or approximate all the wavelengths shown in Fig. 9. Another group of lasers, the semiconductor lasers, provide wavelengths ranging from about 400 nm to 30 μm and typically with very low noise and good power levels, especially in the spectral region from 0.6 to 2.0 μm, though these semiconductor lasers can generate virtually any wavelength. Hence, the 0.5- and 1.5-μm wavelengths used in Fig. 9 may be readily provided by semiconductor lasers. The semiconductor lasers are also attractive owing to their tunability (i.e. to avoid interference from vapor absorption) and relatively low cost. Besides the gas and semiconductor lasers, other common laser devices commercially available include solid-state and dye lasers, whose output wavelengths range typically from about 200 nm to 3.9 mm and from about 300 nm to 750 nm, respectively. These laser devices provide a great many wavelengths in a wide spectral range and will significantly enhance the development of the WMLE technique.

5 Extension to other aerosol systems

Discussions in the preceding sections are based on water aerosols at a temperature of 22°C. This section considers the development of WMLE schemes for the measurement of SDFs for other aerosol systems, including aerosols at different temperatures or aerosols of other liquids such

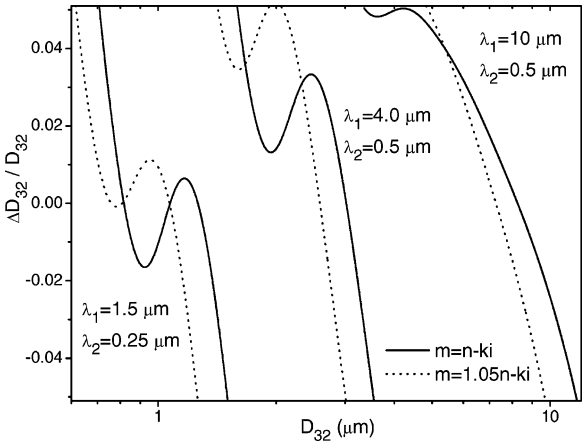

FIGURE 11 Evaluation of the influence of refractive indices on the applicable ranges of the WMLE scheme for D_{32} measurements

as hydrocarbon fuels. This consideration is essentially the consideration of the impact of refractive indices ($m = n - ki$) on the wavelength- selection process for the WMLE scheme and requires studies of the dependence of extinction coefficients on the refractive indices. At wavelengths where the imaginary part of the refractive index of the aerosols is not very large (such as for water aerosols in the wavelength range from 0.25 to 10 μm), the dependence of the Q and $\bar{Q}$ curves on the imaginary part can be neglected. Our calculations show that varying the imaginary part of the refractive indices used in this work by ±25% has a negligible influence on the wavelength-selection process. However, the Q and $\bar{Q}$ curves demonstrate a sensitive dependence on the real part of the refractive indices. A small increase in the real part of the refractive indices causes the Q and $\bar{Q}$ curves to be obviously compressed towards smaller D_{32}, and vice versa. This effect is illustrated in Figs. 11 and 12 by repeating the calculations performed in Figs. 5 and 8 with the real parts of all the refractive indices used in the calculations in Figs. 5 and 8 increased by 5%. Both Figs. 11 and 12 show an overall shift of all the new calculations (performed at $m = 1.05n - ki$) towards smaller D_{32} compared with the calculations performed at $m = n - ki$. This effect suggests that when applied

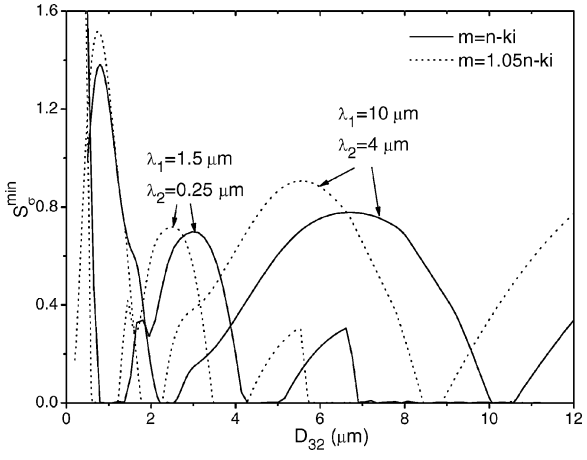

FIGURE 12 Evaluation of the influence of refractive indices on the applicable ranges of the WMLE scheme for distribution width measurements

to aerosols with the real part of the refractive indices larger than that of water aerosols at 22°C (e.g. water aerosols at a temperature lower than 22°C or aerosols of some hydrocarbon fuels), the applicable range of the WMLE scheme described in Fig. 9 is shifted towards smaller D_{32}. On the contrary, when applied to aerosols with the real part of the refractive indices smaller than that of water aerosols at 22°C, the applicable range of this scheme is shifted towards larger D_{32}.

The impact of the aerosol temperature on the WMLE scheme merits more consideration. The above discussions suggest that SDF measurements by the extinction method depend on the aerosol temperature. This dependence generally renders it necessary to know the aerosol temperature and the refractive indices (especially the real part) at this temperature for the extinction method to measure SDFs accurately. On the other hand, this dependence has the potential to allow nonintrusive measurements of the mean aerosol temperature by the WMLE scheme, which is a critical diagnostic need in many fields of aerosol-related research. These measurements of course require the SDF of the aerosols to be well characterized and the relationship between the refractive indices and the aerosol temperature to be well understood. The refractive indices of different liquids exhibit different levels of sensitivity to the liquid temperature. For example, the real part of the refractive index of liquid water varies by 0.8% in a temperature range of 20 to 80°C at wavelengths in the visible range [12, 13]. A similar level of variation is expected at other wavelengths ranging from 0.2 to 10 μm based on the work in Refs. [14, 15], except at those wavelengths where a strong absorption band occurs. Such a variation in the refractive index is substantially smaller than the variation of 5% considered in Figs. 11 and 12. Therefore, the WMLE scheme shown in Fig. 9 should allow measurement of SDFs for water aerosols with reasonable accuracy in this temperature range without detailed knowledge of the aerosol temperature. For liquids whose refractive index varies with temperature more drastically (e.g. some hydrocarbon fuels [13, 16]), application of the WMLE scheme may require more specific information about the aerosol temperature to ensure the accuracy of the SDF measurements. On the other hand, in such cases the WMLE scheme may have the potential to provide sensitive aerosol temperature measurements.

Finally, we consider the extension of applying the WMLE scheme to aerosol systems containing both aerosols and absorbing vapor constituents. Simultaneous characterization of aerosols and vapor using WMLE will be discussed elsewhere. Here we focus our discussion on the uncertainties in SDF measurements due to interference absorption of the laser radiation by vapor constituents. Firstly, the wavelengths in the WMLE scheme can be tuned or replaced by other wavelengths nearby to avoid interference vapor absorption, especially for any vapor constituent (e.g. water vapor) which has discrete and narrow absorption spectral features. In the case where the interference absorption from vapor cannot be avoided, the bounds of uncertainties in the SDF measurements due to vapor interference can be estimated by similar analysis used to generate Fig. 10. More specifically, first, extinction by aerosols and interference absorption by vapor at each wavelength need to be estimated. Second, interference vapor absorption is translated to uncertainties in

ratios of extinction (R's) and then converted to uncertainties in D_{32} measurements using similar calculations shown in Fig. 3. Finally, uncertainties in D_{32} measurements are used to determine the uncertainties in the distribution width.

6 Extension to other distribution functions

This section extends the application of the above method for SDF measurements from the log-normal distribution function to other distribution functions. Application of this SDF measurement method to other two-parameter distribution functions (such as the normal distribution function and the Rosin–Rammler distribution function) is very similar to that for the log-normal distribution function. Combinations of certain wavelengths are found to demonstrate low sensitivity to the detailed shape of the distribution functions to be measured and high sensitivity to D_{32} in certain ranges of D_{32}, and therefore can be used to determine D_{32} in the corresponding range without knowing the exact shape of the distributions. Uncertainties in the determination of D_{32} can be estimated by the methodology described in Sect. 3 and used to specify the applicable ranges of the wavelength combinations. After D_{32} is measured, the shape of the distribution can be determined by combinations of selected wavelengths at which the ratio of mean extinction coefficients is sensitive to the shape of the distribution, similar to the method discussed in Sect. 4.

Here we focus our discussion on the extension of this SDF measurement method to the upper limit distribution function (ULDF) as introduced in Ref. [17], which is a three-parameter distribution function defined as follows:

$$f(D) = B\frac{\exp\left[-\left(\delta \ln\frac{aD}{D_\infty - D}\right)^2\right]}{D^4(D_\infty - D)}, \tag{11}$$

where a and δ are the shape parameters of the distribution, D_∞ is the largest diameter in the distribution, and B is a normalization constant such that the distribution function is normalized, i.e. $\int_0^{D_\infty} f(D)\,\mathrm{d}D = 1$.

The three parameters in the ULDF (a, δ, and D_∞) can be adjusted independently to vary the mean size, the distribution width, and the skewness of the distribution. Figure 13 shows four ULDFs at various a's and δ's (the values of the a's and δ's are listed in the caption) with the same D_∞. Since the shape parameters (a and δ) give no apparent interpretation for the geometrical form of the distributions, Deiss [18] suggested the use of two nondimensional factors, a width factor (W_D) and a skewness factor (S) as defined in Eqs. (12) and (13), to describe the ULDFs:

$$W_\mathrm{D} = \omega/\bar{D}, \tag{12}$$

$$S = \bar{D}/D_\infty, \tag{13}$$

where $\bar{D}$ = the most probable diameter in the distribution as shown in Fig. 13 ω = the width of the distribution at the two diameters (D^+ and D^- in Fig. 13), where the value of $f(D)$ is
half that of $f(\bar{D})$.

According to the definition in Eq. (13), a larger S corresponds to a distribution with modal diameter closer to D_∞ and vice versa. We modify the definition of the width factor defined in Eq. (12) to the following one:

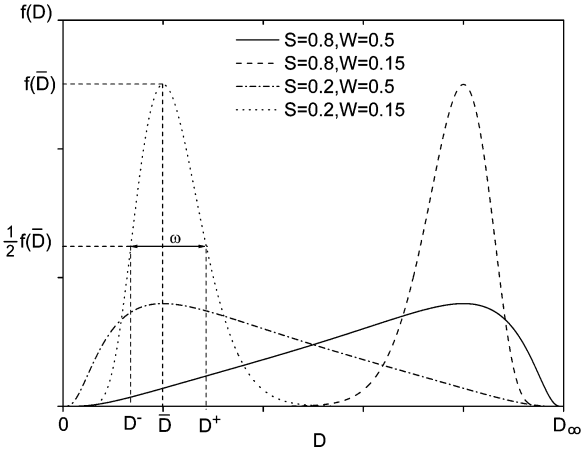

FIGURE 13 Four example ULDFs with different skewnesses and widths. The shape parameters are $a = 0.25$ and $\delta = 0.88$ for $S = 0.8$ and $W = 0.5$, $a = 0.25$ and $\delta = 1.89$ for $S = 0.8$ and $W = 0.15$, $a = 0.57$ and $\delta = 0.88$ for $S = 0.2$ and $W = 0.5$, and $a = 2.63$ and $\delta = 1.89$ for $S = 0.2$ and $W = 0.15$

$$W = \omega/D_\infty. \tag{14}$$

Obviously, W is simply the product of W_D and S; however, a larger W defined in Eq. (14) always corresponds to a distribution with wider half width and vice versa, which is not true for the W_D defined in Eq. (12). Either the shape parameters (a and δ) or the nondimensional factors (W and S) can fully specify the shape of a ULDF and this work uses the nondimensional factors. The nondimensional width and skewness factors are related to the shape parameters through a set of transcendental equations [19], and they are calculated for the distributions presented in Fig. 13. The geometrical forms of the distributions displayed in Fig. 13 suggest that ULDFs with S and W in the range of 0.2 to 0.8 and 0.15 to 0.5, respectively, represent a relatively wide class of distributions in terms of distribution width and skewness. Finally, the Sauter mean diameter (D_{32}) of a ULDF is related to the parameters of the distribution by [17]

$$D_{32} = \frac{D_\infty}{1 + a\exp(1/4\delta^2)}. \tag{15}$$

Figure 14 shows the calculations of mean extinction coefficients ($\bar{Q}$ at three wavelengths for water aerosols following the upper limit distributions specified in Fig. 13. Similar to the observations made in Fig. 2, $\bar{Q}$ at each wavelength shows low sensitivity to the shape of the distribution functions in certain D_{32} ranges, and the same analysis performed in Sect. 2 applies here to explain this low sensitivity. For example, the variations in $\bar{Q}$ at 10 μm remain small over the entire D_{32} range shown in Fig. 14, even if the distributions have quite different shapes, and the variations in $\bar{Q}$ at 0.5 μm start to be damped out after a D_{32} of 4 μm. Therefore, the ratio (R) between $\bar{Q}$ at 10 and at 0.5 μm (R) will be insensitive to the shape of the distributions and can be used to measure D_{32} ranging from 4 to 12 μm without detailed knowledge of the shape parameters (or, equivalently, the nondimensional factors) of the distribution. Ambiguity will occur in the determination of D_{32} because of the lack of knowledge about

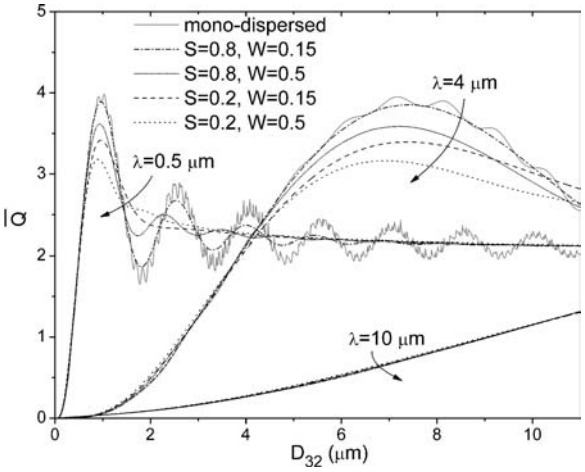

FIGURE 14 $\bar{Q}$ at different wavelengths for water aerosols at a temperature of 22°C following the ULDFs specified in Fig. 13

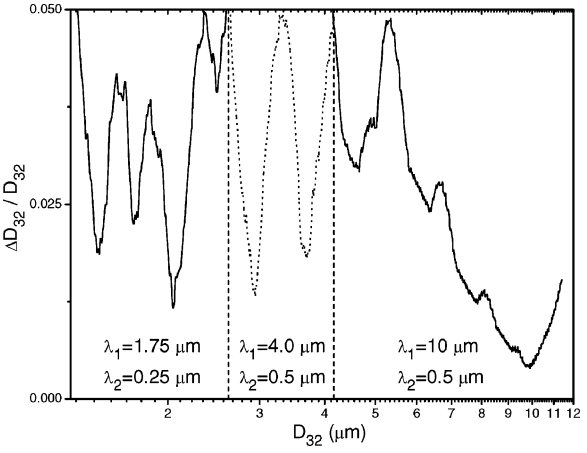

FIGURE 15 Wavelengths selected for the measurement of D_{32} of water aerosols following ULDFs with W and S in the ranges of 0.15 to 0.5 and 0.2 to 0.8, respectively

the shape parameters, and this ambiguity is still quantified by $\Delta D_{32}/D_{32}$ defined in Eq. (8). However, here the definitions of D_{32}^1 and D_{32}^2 need to be modified to be the largest and smallest possible D_{32} determined by R curves between a pair of wavelengths in the W and S ranges under consideration, and $\Delta D_{32}/D_{32}$ is always positive under these modified definitions.

Figure 15 shows the calculation of $\Delta D_{32}/D_{32}$ when R, the ratio of measured extinction at 10 and 0.5 μm, is used to determine D_{32} between $\bar{Q}$ at 10 and 0.5 μm is used to determine D_{32} for water aerosols following upper limit distributions with W and S in the ranges of 0.15 to 0.5 and 0.2 to 0.8, respectively. As expected from the above analysis of $\bar{Q}$, the combination of these two wavelengths enables measurements of D_{32} within 5% for 4.2 μm $< D_{32} <$ 12 μm. Other wavelengths can be selected to measure D_{32} in other ranges. For example, Fig. 15 shows that a wavelength combination of 4 and 0.5 mm enables determination of D_{32} within 5% for 2.6 μm $< D_{32} <$ 4.2 μm, and a combination of 1.75 and 0.25 μm for 1.3 μm $< D_{32} <$ 2.6 μm. Similar to the discussions of the measurements of D_{32} for log-normal distributions, more wavelengths can be incorporated to enable the measurement of D_{32} with smaller ambiguity and to expand the measurements to wider ranges of D_{32}, W, and S. Moreover, the influence of refractive index on the D_{32} measurements also has the same trend as that analyzed in the case of log-normal distributions.

However, the determination of the shape parameters of the ULDFs after D_{32} has been measured requires a different method than that developed for the two-parameter distributions. The reason is that no such wavelength can be found at which $\bar{Q}$ is sensitive to one of the shape parameters but insensitive to the other, which is illustrated by calculations of $\bar{Q}$ in Fig. 14. Consequently, the influence of the shape parameters on $\bar{Q}$ cannot be decoupled and determined separately. An optimization method [11] or a matrix inversion method [1] can be applied here to solve for the shape parameters. But, the methodology developed in Sect. 4 for the evaluation of sensitivity of $\bar{Q}$ to the shape parameters still applies here and would provide useful guidance to determine the application ranges of different wavelengths to achieve optimum measurement sensitivity and accuracy.

7 Summary and discussions

Strategies based on WMLE for SDF measurements have been introduced and developed for a variety of distribution functions. Incorporation of wavelengths from a wide spectral range in the WMLE scheme was demonstrated to enable a stable inversion of the extinction measurements to SDFs with enhanced accuracy. Sensitivity analysis reveals the proper ranges over which the extinction measurements at the wavelengths selected in the WMLE scheme should be applied for optimized sensitivity and accuracy of the SDF measurements. The analysis performed here should provide theoretical support for the practical implementation of the WMLE concept, and motivate further research work on the development of such a concept.

Moreover, by incorporation of additional wavelengths to monitor the spectral absorption by the vapor in association with the aerosols, the WMLE scheme can be extended to enable simultaneous measurements of multiple quantities both of the aerosols and of the vapor, including the SDF and loading of the aerosols, and the concentration and temperature of the vapor. These developments underway will further increase the capabilities of the WMLE technique.

ACKNOWLEDGEMENTS Special thanks are due to Thomas C. Hanson and David F. Davidson for many valuable discussions and assistance in the demonstration of the WMLE scheme in the aerosol shock tube facility. This research was supported by the US Air Force Office of Scientific Research, Aerospace Sciences Directorate, with Dr. Julian Tishkoff as technical monitor, and the Global Climate and Energy Project (GCEP) at Stanford University.

REFERENCES

1 P.T. Walters, Appl. Opt. **19**, 2353 (1980)
2 G. Ramachandran, D. Leith, Aerosol Sci. Technol. **17**, 303 (1992)
3 S. Twomey, H.B. Howell, Appl. Opt. **6**, 2125 (1967)
4 H.J. Smolders, M.E.H. van Dongen, Shock Waves **2**, 255 (1992)
5 M.E.H. van Dongen, H.J. Smolders, C.J.M. Braun, C.A.M. Snoeijs, J.F.H. Willems, Appl. Opt. **33**, 1980 (1994)
6 K.S. Shifrin, I.G. Zolotov, Appl. Opt. **36**, 6047 (1997)
7 K.S. Shifrin, I.G. Zolotov, Appl. Opt. **35**, 2114 (1996)
8 P.C. Hansen, Inverse Probl. **8**, 849 (1992)
9 L.D. Kou, D. Labrie, P. Chylek, Appl. Opt. **32**, 3531 (1993)
10 G.M. Hale, M.R. Querry, Appl. Opt. **12**, 555 (1973)

11 X.S. Cai, N.N. Wang, J.M. Wei, G. Zheng, J. Aerosol Sci. **23**, 749 (1992)
12 C.H. Cho, J. Urquidi, G.I. Gellene, G.W. Robinson, J. Chem. Phys. **114**, 3157 (2001)
13 D.R. Lide, H.P.R. Frederikse (eds.), *CRC Handbook of Chemistry and Physics*, 76th edn. (CRC, Boca Raton, FL, 1995)
14 P. Schiebener, J. Straub, J.M.H.L. Sengers, J.S. Gallagher, J. Phys. Chem. Ref. Data **19**, 677 (1990)
15 L.W. Pinkley, P.P. Sethna, D. Williams, J. Opt. Soc. Am. **67**, 494 (1997)
16 J.A. Drallmeier, J.E. Peters, Appl. Opt. **29**, 1040 (1990)
17 R.A. Mugele, H.D. Evans, Ind. Eng. Chem. **43**, 1317 (1951)
18 W.E. Deiss, *The Optical Determination of Particle Sizes Obeying the Upper Limit Distribution Function*, Senior Thesis, Princeton University (1960)
19 J.H. Roberts, M.J. Webb, AIAA J. **2**, 583 (1964)